Inorganic Chemistry

Article

pubs.acs.org/IC

A Single-Component White-Emitting $CaSr_2Al_2O_6:Ce^{3+}$, Li^+, Mn^{2+} Phosphor via Energy Transfer

Yanyan Li, Yurong Shi, Ge Zhu, Quansheng Wu, Hao Li, Xicheng Wang, Qian Wang, and Yuhua Wang*

Key Laboratory for Special Function Materials and Structural Design of the Ministry of Education, School of Physical Science and Technology, Lanzhou University, Lanzhou, 730000, China

Supporting Information

ABSTRACT: A series of single-component Ce^{3+}, Li^+, Mn^{2+} ions codoped color-tunable $CaSr_2Al_2O_6$ phosphors were synthesized by a high-temperature solid-state reaction, and the photoluminescence properties as well as the energy transfer mechanism from Ce^{3+} to Mn^{2+} ions have been investigated in detail. The Ce^{3+} activated phosphors have strong absorption in the range of 250−420 nm and can give a blue emission centered at about 460 nm. When Mn^{2+} ions are codoped, the emission of $CaSr_2Al_2O_6:Ce^{3+}$, Li^+, Mn^{2+} phosphors can be tuned from blue to red through adjusting the doping concentration of the Mn^{2+} ions, under the irradiation of 358 nm. When the concentration of Mn^{2+} is increased to 0.02, a warm-white light can be obtained with good CIE coordinates of (0.388, 0.323) and a low CCT of 3284 K. The energy transfer mechanism from the Ce^{3+} to Mn^{2+} ions is demonstrated to be a quadrupole−quadrupole interaction based on the analysis of the decay curves of the phosphors. The thermal quenching stability was also investigated. The results indicate that $CaSr_2Al_2O_6:Ce^{3+}$, Li^+, Mn^{2+} samples might have potential applications in *w*-LEDs.

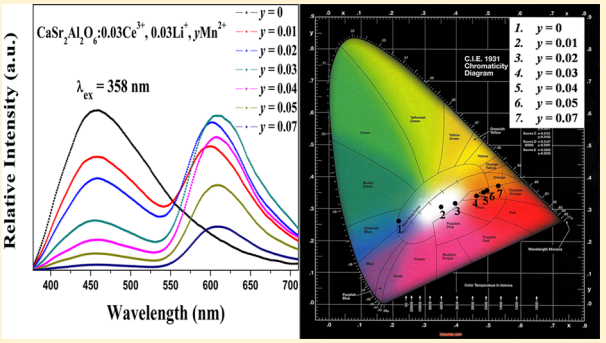

INTRODUCTION

Compared with the traditional incandescent and fluorescent lamps, white-light-emitting diodes (*w*-LEDs) possess merits of high efficiency, long lifetime, and environmental friendliness and have become another trend for general illumination.[1−4] Currently, the commercial *w*-LEDs are based on a blue InGaN LED chip that excites a yellow-emitting phosphor $(Y,Gd)_3(Al,Ga)_5O_{12}:Ce^{3+}$ (YAG:Ce). However, YAG:Ce has a deficient red emission, leading to its bluish-cold light owing to its high color temperature (CCT > 4500 K) and low color rendering index (CRI ≈ 70−80). Such high CCT and low CRI cannot meet the requirements for many sophisticated applications, such as light sources in offices, schools, medicals, hospitals, and hotels.[5−7] Recently, utilizing an ultraviolet (UV) LED chip to excite blends of blue-, green-, and red-emitting phosphors has been employed to solve the above problems. This combination can produce warm-white light with excellent CRI.[8] Unfortunately, the strong reabsorption of the blue-light by the green and red phosphors significantly lowers the conversion efficiency of the device and different degradation rates of the three-primary phosphors will cause color aberration, which is undesirable in practice.[9−11]

In recent years, single-component white light/full color emission phosphors realized by energy transfer from the sensitizer to the activator in a proper host have attracted significant interest due to their good luminescence efficiency, color reproducibility, and low manufacturing costs.[12] Mn^{2+}-doped luminescent materials have been known to have wide-range emissions from 500 to 700 nm depending on the crystal field of the host material.[13−15] Mn^{2+} ions are good candidates for green (weak crystal field) and red (stronger crystal field) phosphors, but the disadvantage of them is that the *d*−*d* absorption transition is difficult to pump, since it is both parity and spin forbidden. As a promising sensitizer for Mn^{2+} ions, Ce^{3+} ions have been widely applied in many Mn^{2+}-doped hosts, such as $Ca_3Sc_2Si_3O_{12}$,[16] $KBaY(BO_3)_2$,[17] $Ca_2Gd_8(SiO_4)_6O_2$,[18] and $Ca_9Al(PO_4)_7$,[19] to improve the emission intensity of Mn^{2+}.

The crystal structure of $CaSr_2Al_2O_6$ was first reported by Walz.[20] $CaSr_2Al_2O_6$ crystallizes in the cubic space group $Pa\bar{3}(205)$ with unit cell dimensions of $a = b = c = 15.55$ Å, and $Z = 24$. Moreover, there are six different crystallographic sites that are available for Ca^{2+} and Sr^{2+} ions in the host lattice. It is well-known that the aluminate compounds including alkaline earth ions provide suitable host lattices for the luminescence of various rare earth ions,[21−23] thus codoping Ce^{3+} and Mn^{2+} into such a host may hopefully generate color tunable lights including white light emission, where the Ce^{3+} ion probably acts as an efficient sensitizer that transfers energy to the Mn^{2+} ion. In addition, analyzing the location of doping ions in a specific host has always been a confused issue for researchers to provide the explanation of the intrinsic mechanism of the luminescent materials.

Received: April 26, 2014
Published: June 26, 2014

   dx.doi.org/10.1021/ic500963q | *Inorg. Chem.* 2014, 53, 7668−7675

In this work, we investigated the crystallographic cation sites occupancy, luminescence properties, and the energy transfer mechanism from the Ce^{3+} to Mn^{2+} ions of $CaSr_2Al_2O_6$:Ce^{3+}, Li^+, Mn^{2+} phosphors. The occupancy of Ce^{3+} ions on different cation sites was discussed in detail, and tunable colors including warm-white emission can be obtained by adjusting the ratio of Ce^{3+} and Mn^{2+} ions in $CaSr_2Al_2O_6$. The results indicate that the $CaSr_2Al_2O_6$:Ce^{3+}, Li^+, Mn^{2+} phosphor might have potential applications as a single-component white-emitting phosphor for UV-excited *w*-LEDs.

EXPERIMENTAL SECTION

Samples of $CaSr_2Al_2O_6$:xCe^{3+}, xLi^+ ($0.01 \le x \le 0.09$) and $CaSr_2Al_2O_6$: $0.03Ce^{3+}$, $0.03Li^+$, yMn^{2+} ($0 \le y \le 0.07$) investigated in this work were synthesized through solid-state reactions. $CaCO_3$ (A.R.), $SrCO_3$ (A.R.), Al_2O_3 (A.R.), CeO_2 (99.999%), and $MnCO_3$ (A.R.) were employed as raw materials. To avoid the charge unbalance and formation of vacancies caused by Ce^{3+} substituting Ca^{2+} or Sr^{2+}, Li_2CO_3 (A.R.) was added as a charge compensator. These raw materials in the desired ratio were mixed in an agate mortar by adding an amount of ethanol and then grinded for 30 min. Finally, the mixture was placed into alumina crucibles and then fired at 1400 °C for 6 h under a reductive atmosphere (10% H_2 + 90% N_2). After firing, the samples were cooled to room temperature in the furnace and ground again into powder for subsequent use.

All the phase structures of samples were characterized by powder X-ray diffraction (XRD) using a Rigaku diffractometer with Ni-filtered Cu Kα radiation. The diffuse-reflectance spectrum (DRS) was obtained by a UV−visible spectrophotometer (PE Lambda 950) using $BaSO_4$ as a reference. The photoluminescence (PL) and PL excitation (PLE) spectra were obtained by a FLS-920 T fluorescence spectrophotometer equipped with Xe 900 (450 W xenon arc lamp) as the light source. The PL decay curves were measured by a FLS-920T fluorescence spectrophotometer with an nF900 ns Flashlamp as the light source. All the above measurements were performed at room temperature. High-temperature luminescence intensity measurements were carried out by using an aluminum plaque with cartridge heaters; the temperature was measured by thermocouples inside the plaque and controlled by a standard TAP-02 high-temperature fluorescence controller.

RESULTS AND DISCUSSION

Crystal Structure of $CaSr_2Al_2O_6$. Figure 1 shows the selected XRD patterns of the as-synthesized $CaSr_2Al_2O_6$: $0.03Ce^{3+}$, $0.03Li^+$ and $CaSr_2Al_2O_6$:$0.03Ce^{3+}$, $0.03Li^+$, yMn^{2+} ($0.01 \le y \le 0.07$) phosphors, which match well with JCPDS file No. 52-0249. The XRD patterns of $CaSr_2Al_2O_6$:xCe^{3+}, xLi^+ ($0.01 \le y \le 0.09$) are shown in the Supporting Information, Figure S1. The crystal structure of $CaSr_2Al_2O_6$, which is according to the previously reported crystallographic data (ICSD # 406613),[20] is shown in Figure 2a. In this structure,

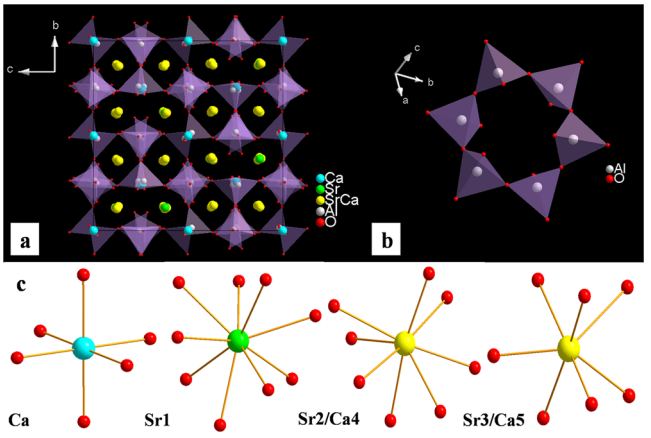

Figure 2. (a) The framework of $CaSr_2Al_2O_6$ viewed along [100]. (b) Corrugated 6-membered ring structure. (c) The coordination environment of cations in the host (Ca1, Ca2, and Ca3 are all six-coordinated).

$[AlO_4]$ tetrahedrons construct highly corrugated 6-membered rings rather than the $[AlO_4]_n$ layers, which is shown in Figure 2b. The tetrahedrons connect with each other by sharing O atoms on bridging positions. Six different crystallographic sites are available for Ca^{2+} and Sr^{2+} ions. Ca1, Ca2, and Ca3 are six-coordinated with similar Ca−O distances, while Sr1, Sr2/Ca4, and Sr3/Ca5 are nine-, eight-, and seven-coordinated, respectively.[20] Table 1 lists the ionic radii[24] of different cations, and the Ce^{3+} and Mn^{2+} ions were expected to occupy the Ca^{2+} or Sr^{2+} sites in view of the similar ionic radii and valence states.

Table 1. Ionic Radii (Å) of Different Cations for the Given Coordination Number (CN)

	ionic radii (Å)			
ion	CN = 6	CN = 7	CN = 8	CN = 9
Ce^{3+}	1.01	1.07	1.143	1.196
Mn^{2+}	0.83	0.90	0.96	
Ca^{2+}	1.00	1.06	1.12	1.18
Sr^{2+}	1.18	1.21	1.26	1.31

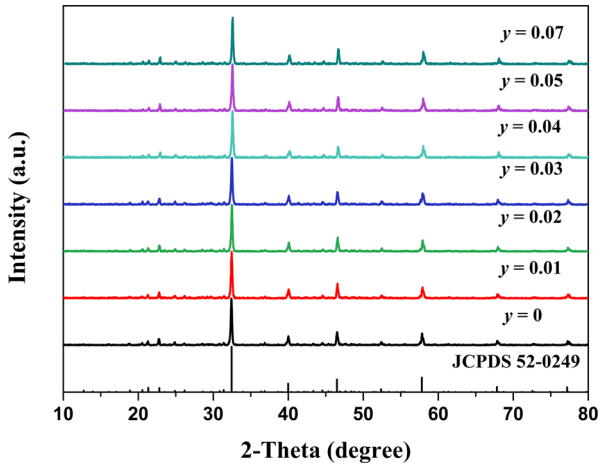

Figure 1. XRD patterns for $CaSr_2Al_2O_6$:$0.03Ce^{3+}$, $0.03Li^+$, yMn^{2+} ($0 \le y \le 0.07$) samples and the standard data for $CaSr_2Al_2O_6$ (JCPDS No. 52-0249).

Photoluminescence Properties of $CaSr_2Al_2O_6$:Ce^{3+}, Li^+. Figure 3 shows the PL and PLE spectra of $CaSr_2Al_2O_6$: $0.03Ce^{3+}$, $0.03Li^+$. The excitation spectrum of the sample consists of three broad excitation bands peaking at 310, 358, and 397 nm, which corresponds to electron transitions of the Ce^{3+} ions from the 4*f* ground state to the different components of excited 5*d* states split by the crystal field. Under optimal excitation wavelength at 358 nm, the sample exhibits a blue emission band with maximum emission at 460 nm, which originates from the 5*d*−4*f* transition of Ce^{3+} ions. Figure 4 depicts the PL and PLE spectra of $CaSr_2Al_2O_6$:xCe^{3+}, xLi^+ ($0.01 \le x \le 0.09$). The Ce^{3+} ions emission bands show a red-shift behavior from 438 nm for x = 0.01 to 470 nm for x = 0.09,

dx.doi.org/10.1021/ic500963q | Inorg. Chem. 2014, 53, 7668−7675

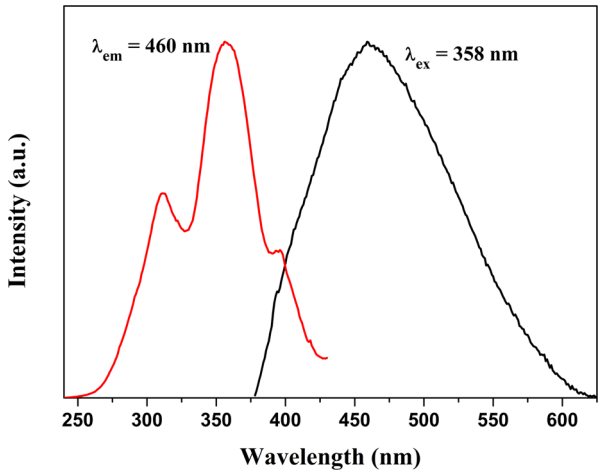

Figure 3. PL and PLE spectra of $CaSr_2Al_2O_6$:0.03Ce^{3+}, 0.03Li^+.

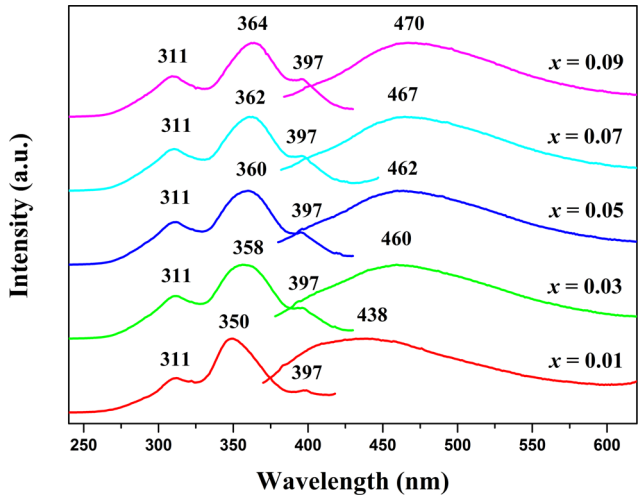

Figure 4. PL and PLE spectra of $CaSr_2Al_2O_6$:Ce^{3+} with varying doped Ce^{3+} concentrations.

which can be attributed to two factors: reabsorption of the high energy emission and different preference for Ce^{3+} to occupy different cation sites. As shown in Figure 4, the excitation and emission spectra overlap with each other to some extent, which indicates that the reabsorption mechanism may play a role in energy transfer of Ce^{3+}-doped $CaSr_2Al_2O_6$ phosphors, which further results in the red shift of the emission bands.[25] However, the shape of the emission spectrum for x = 0.01 is obviously different from that of the others, which may be resulted from different preference for Ce^{3+} to replace different cation sites.

As mentioned above, six different crystallographic sites are available for Ca^{2+} and Sr^{2+} ions. According to ref 19, Ca1, Ca2, and Ca3 are all six-coordinated and there are few differences among the three sites, which may make the emission peaks of Ca1, Ca2, and Ca3 undistinguished. In order to simplify the discussion of the emission originated from different cation sites, here, we do not distinguish the emission peaks of Ce^{3+} occupying Ca1, Ca2, and Ca3 and regard them as the whole emission of Ce^{3+} occupying Ca^{2+} sites. Therefore, the emission peaks of Ce^{3+} can be originated from four different sites: (Ca1, Ca2, Ca3), Sr1, Sr2/Ca4, and Sr3/Ca5, which are named as M1, M2, M3, and M4, respectively. Moreover, the order of the average bond lengths R for the four sites is[20] R(M2−O) > R(M3−O) > R(M4−O) > R(M1−O).

It is accepted that the emission of Ce^{3+} ions can be attributed to the transitions from the lowest 5d excited state to the $^2F_{5/2}$ and $^2F_{7/2}$ ground states, which results in the fact that two distinguished emission spectra with a theoretical energy value of about 2000 cm^{-1} can be decomposed. Accordingly, the emission bands of $CaSr_2Al_2O_6$:0.01Ce^{3+}, 0.01Li^+ and $CaSr_2Al_2O_6$:0.03Ce^{3+}, 0.03Li^+ are decomposed into eight well-separated Gaussian components (in Figure 5) with maxima

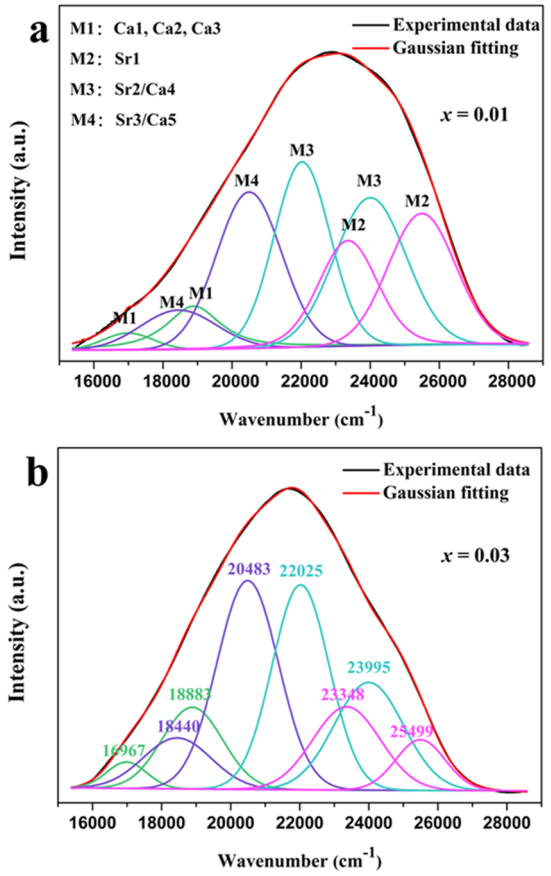

Figure 5. Gaussian fitting of the emission bands of (a) $CaSr_2Al_2O_6$: 0.01Ce^{3+}, 0.01Li^+ and (b) $CaSr_2Al_2O_6$:0.03Ce^{3+}, 0.03Li^+ (λ_{ex} = 358 nm).

wavenumbers at 16967 and 18883 cm^{-1}, 18440 and 20483 cm^{-1}, 22025 and 23995 cm^{-1}, and 23348 and 25499 cm^{-1}, respectively. The above values can be divided into four groups according to the calculated Gaussian wavenumbers (Table 2), which further verifies that Ce^{3+} will occupy four different Ca^{2+} or Sr^{2+} sites in the present $CaSr_2Al_2O_6$ host.

The position of the emission peak is highly dependent on the crystal field strength of the activators. The relation between the crystal field strength (D_q) and R is expressed as the following equation[26]

$$D_q \propto \frac{1}{R^5} \quad (1)$$

where R is the distance between the central ion and its ligands. It can be seen from eq 1 that D_q is inversely proportional to the fifth power of the bond length R. Because the average distance of Ce_M−O for Ce_{M1}−O is the shortest, the crystal field strength of Ce^{3+} at M1 site is larger than that at M2, M3, and M4 sites.

dx.doi.org/10.1021/ic500963q | Inorg. Chem. 2014, 53, 7668−7675

Table 2. Gaussian Fitting Results for the Four Different Sites

site	M1		M2		M3		M4	
wavenumber (cm^{-1})	16967 (589 nm)	18883 (529 nm)	23348 (428 nm)	25499 (392 nm)	22025 (454 nm)	23995 (417 nm)	18440 (542 nm)	20483 (488 nm)

Therefore, the lowest excited state of the Ce^{3+} ion at M1 site is lower in energy than that at M2, M3, and M4 sites. Hence, it is deduced that the lowest-energy (16967 and 18883 cm^{-1}) peaks are assigned to the transitions of Ce^{3+} ions occupying the M1 site. Moreover, according to the order of the average bond lengths mentioned above, it can be deduced that the 18440 and 20483 cm^{-1}, 22025 and 23995 cm^{-1}, and 23348 and 25499 cm^{-1} peaks are assigned to transitions at Ce^{3+} ions occupying sites M4, M3, and M2, respectively, which are listed in Table 2.

It can be seen from Figure 5 that, when the concentration of Ce^{3+} is equal to 0.01, Ce^{3+} ions prefer to occupy the larger M2 site. However, when $x = 0.03$, the preference for Ce^{3+} ions to occupy the M2 site is reduced and thus results in the difference of the emission spectra shapes for $x = 0.01$ and $x = 0.03$. When $x \geq 0.03$, the emission spectra have the similar shapes. Therefore, we can conclude that, when x increases from 0.01 to 0.03, the preference for Ce^{3+} ions to occupy different sites could be the dominant reason for the red shift of the emission spectra. However, when $x \geq 0.03$, the mechanism of reabsorption could be the dominant reason for the red shift of the emission spectra.

Figure S2 (as shown in the Supporting Information) shows the PL intensity of $CaSr_2Al_2O_6$:$x$$Ce^{3+}$, $x$$Li^+$ as a function of doped Ce^{3+} concentration. The optimal doping concentration was observed to be $x = 0.03$. The PL intensity was found to decline dramatically as the concentration of Ce^{3+} exceeds $x = 0.03$ due to concentration quenching. According to the Dexter's energy transfer theory,[27] concentration quenching is mainly caused by the nonradiative energy migration among the Ce^{3+} ions at the high concentration. The critical distance between the Ce^{3+} ions can be calculated using the following equation[28]

$$R_C = 2 \times \left(\frac{3V}{4\pi x_c Z}\right)^{1/3} \quad (2)$$

where V is the volume of the unit cell, Z represents the formula units per unit cell, and x_c is the critical concentration. By taking the values of $V = 3760.03$ Å^3, $Z = 24$, and $x_c = 0.03$, the critical transfer distance R_C was found to be 21.52 Å. There are two types of energy transfer: one is exchange interaction, and the other one is multipolar interaction.[29,30] In the case of the exchange interaction, the critical distance between the sensitizer and activator is always shorter than 4 Å.[31] Since the critical distance calculated for $CaSr_2Al_2O_6$:Ce^{3+} is much larger than 4 Å, there is little possibility of energy transfer via the exchange interaction mechanism. Consequently, it is the electric multipolar interaction that will take place for energy transfer among Ce^{3+} ions.[32]

Photoluminescence Properties and Energy Transfer in the $CaSr_2Al_2O_6$:Ce^{3+}, Li^+, Mn^{2+} Phosphors. Figure 6a depicts the PLE spectrum of the Mn^{2+} ions singly doped phosphor, as well as the DRS of the $CaSr_2Al_2O_6$ host. While monitoring at 610 nm, a broad band ranging from 240 to 300 nm and five distinct peaks peaked at 352, 367, 419, 435, and 467 nm exist in the excitation spectrum, which are attributed to host lattice absorption (as shown in the DRS spectrum) and Mn^{2+} absorption transitions,[33−35] respectively. The PL

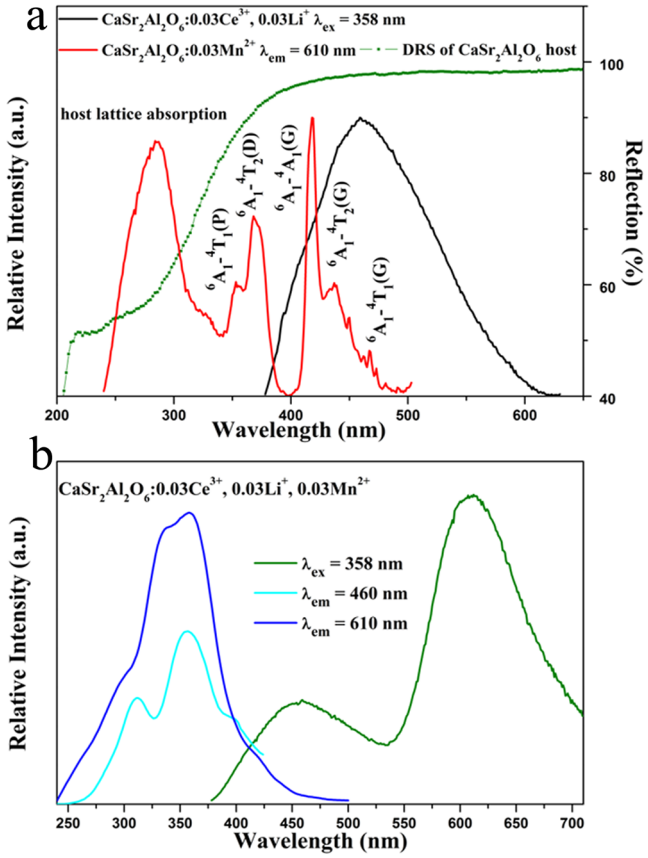

Figure 6. (a) PLE spectrum of Mn^{2+}-doped and PL spectrum of Ce^{3+}-doped $CaSr_2Al_2O_6$, as well as the DRS of undoped $CaSr_2Al_2O_6$. (b) PL and PLE spectra of $CaSr_2Al_2O_6$:0.03Ce^{3+}, 0.03Li^+, 0.03Mn^{2+} phosphor.

spectrum of $CaSr_2Al_2O_6$:0.03Ce^{3+}, 0.03Li^+ is also shown in Figure 6a. A significant spectral overlap between the PL spectrum of $CaSr_2Al_2O_6$:Ce^{3+}, Li^+ and the PLE spectrum of $CaSr_2Al_2O_6$:Mn^{2+} is observed, which indicates that the energy transfer from the Ce^{3+} to Mn^{2+} ions can be expected in Ce^{3+} and Mn^{2+} codoped host. Figure 6b depicts the PL and PLE spectra of the $CaSr_2Al_2O_6$:0.03Ce^{3+}, 0.03Li^+, 0.03Mn^{2+} phosphor. The codoped phosphor shows a blue emission band due to the $5d$−$4f$ transition of Ce^{3+} ions and a red emission band due to the $^4T_1$−$^6A_1$ transition of Mn^{2+} ions at the irradiation of 358 nm. The red emission of Mn^{2+} ions in $CaSr_2Al_2O_6$ indicates that the Mn^{2+} ions occupy the octahedral sites of Ca^{2+} ions, not the tetrahedral sites of Al^{3+} ions, since the Mn^{2+} ions will emit red emission in the octahedral crystal field and give green emission in the tetrahedral crystal field.[33] What can be also seen from Figure 6b is that the excitation spectrum of $CaSr_2Al_2O_6$:0.03Ce^{3+}, 0.03Li^+, 0.03Mn^{2+} monitored at the emission of the Mn^{2+} ions is similar to that monitored at the emission of the Ce^{3+} ions, which strongly validates the occurrence of the energy transfer from the Ce^{3+} to Mn^{2+} ions. The difference between the two excitation spectra may be caused by the effect of the Mn^{2+} ions on the crystal field around the Ce^{3+} ions.[12] Another reason for this phenomenon may be

dx.doi.org/10.1021/ic500963q | Inorg. Chem. 2014, 53, 7668−7675

ascribed to the superposition of the PLE spectra of Ce^{3+} and Mn^{2+} singly doped $CaSr_2Al_2O_6$, for the Mn^{2+}-doped phosphor has absorption around 358 nm.

In order to study the effect of doping concentration of Mn^{2+} ions on the luminescence properties of the phosphors, a series of $CaSr_2Al_2O_6$:0.03Ce^{3+}, 0.03Li^+, yMn^{2+} ($0 \le y \le 0.07$) samples have been prepared. Figure 7 demonstrates the emission

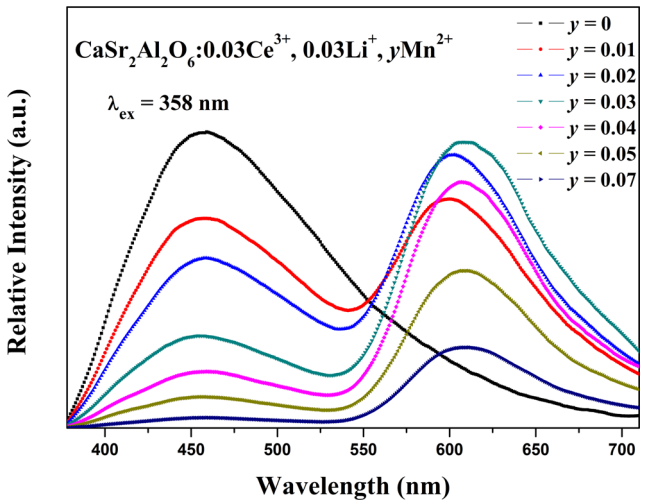

Figure 7. Emission spectra of $CaSr_2Al_2O_6$:0.03Ce^{3+}, 0.03Li^+, yMn^{2+} ($0 \le y \le 0.07$) phosphors.

spectra of the phosphors at the excitation of 358 nm. It can be seen that the emission intensity of the Ce^{3+} ions decreases monotonously with the increment of the Mn^{2+} concentration, whereas the emission intensities of the Mn^{2+} first increase to a maximum at $y = 0.03$ and then decrease due to concentration quenching. The emission colors of $CaSr_2Al_2O_6$:0.03Ce^{3+}, 0.03Li^+, yMn^{2+} phosphors are then tuned from blue to red by adjusting the Mn^{2+} concentration, as expected. From Figure 7, one can also see that the peak positions of Mn^{2+} emission shift to longer wavelengths with an increase of Mn^{2+} concentration. This phenomenon can be ascribed to the increase of the crystal field surrounding the Mn^{2+} ions caused by the substitution of the Ca^{2+} ions by Mn^{2+} ions. Since the ionic radius of the Mn^{2+} ion is much smaller than that of the Ca^{2+} ion, doping of Mn^{2+} will cause shrinkage of the unit cell volume and the length of the Mn−O will become shorter. This variation leads to the increment of the crystal field splitting and further results in the red shifting of the Mn^{2+} emission.[36,37]

In order to further investigate the dynamic luminescence process between Ce^{3+} and Mn^{2+}, the decay curves of Ce^{3+} in the phosphors were measured by monitoring at 460 nm with the irradiation of 358 nm. The fluorescence of Ce^{3+} decays faster and tends to be a nonexponential function with increasing the Mn^{2+} concentration, as shown in Figure 8a. The decay process of these samples is characterized by an average lifetime τ, which can be calculated using eq 3 as follows[38−40]

$$\tau = \frac{\int_{\infty}^{0} I(t)t\ \mathrm{d}t}{\int_{\infty}^{0} I(t)\ \mathrm{d}t} \tag{3}$$

where $I(t)$ is the luminous intensity at time t. On the basis of eq 3, the luminescence lifetimes of Ce^{3+} are determined to be 21.92, 20.57, 20.34, 17.94, 17.49, 16.73, and 16.01 ns for Mn^{2+}

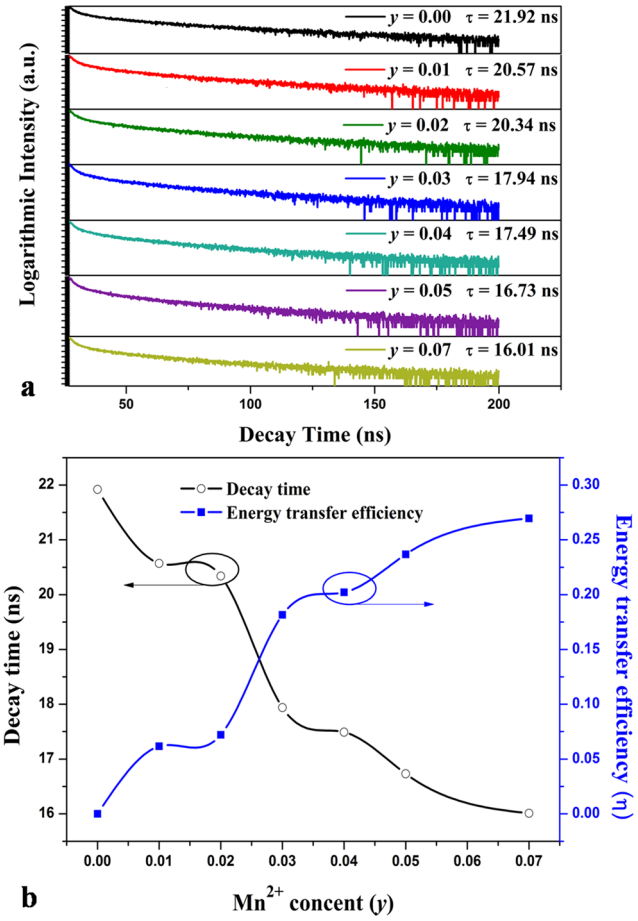

Figure 8. (a) The decay curves for Ce^{3+} in the $CaSr_2Al_2O_6$:0.03Ce^{3+}, 0.03Li^+, yMn^{2+} ($0 \le y \le 0.07$) phosphors, excited at 358 nm and monitored at 460 nm. (b) The fluorescence lifetime of Ce^{3+} ions and energy transfer efficiencies from Ce^{3+} to Mn^{2+} as a function of Mn^{2+} concentration.

concentrations of 0, 0.01, 0.02, 0.03, 0.04, 0.0.05 and 0.07, respectively. The decrease in the lifetimes of Ce^{3+} with increasing Mn^{2+} concentration strongly demonstrates an energy transfer from Ce^{3+} to Mn^{2+}. In addition, the energy transfer efficiency (η) from Ce^{3+} to Mn^{2+} is calculated by the following equation[39,40]

$$\eta = 1 - \tau_s/\tau_{s0} \tag{4}$$

where τ_{s0} and τ_s represent the lifetime of Ce^{3+} in the absence and presence of Mn^{2+}, respectively. As shown in Figure 8b, the energy transfer efficiencies increase gradually with increasing Mn^{2+} concentration and η are calculated to be 0, 6.16, 7.21, 18.16, 20.21, 23.68, and 26.96% for the $CaSr_2Al_2O_6$:0.03Ce^{3+}, 0.03Li^+, yMn^{2+} phosphors with $y = 0$, 0.01, 0.02, 0.03, 0.04, 0.05, and 0.07, respectively.

In general, energy transfer from the sensitizer to activator in a phosphor may take place via a multipolar interaction[41] or an exchange interaction at higher concentrations. On the basis of Dexter's energy transfer expression for multipolar interactions and Reisfeld's approximation,[39,40] the following relationship can be given

$$P_{SA} = \frac{1}{\tau_{s0}} - \frac{1}{\tau_s} \propto C^{n/3} \tag{5}$$

dx.doi.org/10.1021/ic500963q | Inorg. Chem. 2014, 53, 7668−7675

where P_{SA} is the energy transfer probability and C is the concentration of Mn^{2+}. The relationship of $P_{SA} \propto C^{n/3}$, where n = 6, 8, and 10, corresponds to dipole−dipole, dipole−quadrupole, and quadrupole−quadrupole interactions,[41] respectively. Figure 9 depicts the double logarithm plots of $|P_{SA}|$

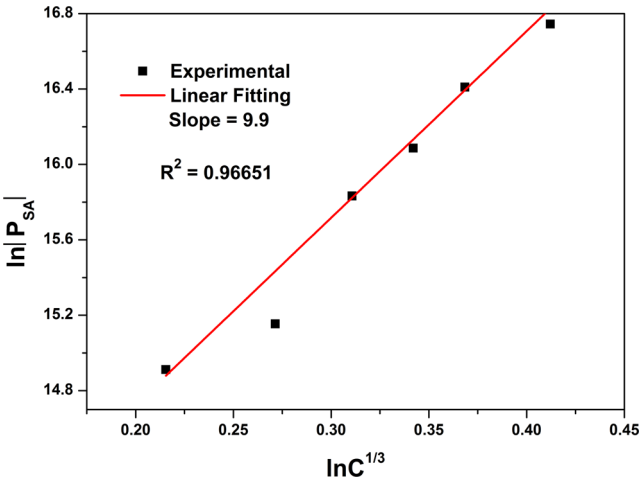

Figure 9. Dependence of $\ln|P_{SA}|$ vs. $\ln(C^{1/3})$ for the $CaSr_2Al_2O_6$:$0.03Ce^{3+}$, $0.03Li^+$, yMn^{2+} $(0.01 \leq y \leq 0.07)$ phosphors.

vs. $C^{1/3}$ for the $CaSr_2Al_2O_6$:$0.03Ce^{3+}$, $0.03Li^+$, yMn^{2+} phosphors $(0.01 \leq y \leq 0.07)$ with a slope of n = 9.9. The value is close to 10, indicating that the dominant energy transfer mechanism in the phosphor system is a quadrupole−quadrupole interaction.

The x and y values of the CIE chromaticity coordinates for the $CaSr_2Al_2O_6$:$0.03Ce^{3+}$, $0.03Li^+$, yMn^{2+} phosphors are calculated and presented in Table 3 and Figure 10, which

Table 3. CIE Coordinates and CCT of $CaSr_2Al_2O_6$:$0.03Ce^{3+}$, $0.03Li^+$, yMn^{2+} Samples

sample no.	Mn^{2+} concentration	CIE coordinates (x, y)	CCT (K)
1	0.00	(0.216, 0.256)	28656
2	0.01	(0.345, 0.306)	4814
3	0.02	(0.388, 0.323)	3284
4	0.03	(0.460, 0.342)	2070
5	0.04	(0.490, 0.355)	1892
6	0.05	(0.502, 0.357)	1824
7	0.07	(0.534, 0.368)	1738

were determined from the corresponding PL spectra at the excitation of 358 nm. By simply varying the concentration of Mn^{2+} ions from 0 to 0.07, tunable colors can be easily obtained under UV irradiation. Accordingly, the CIE coordinates vary from (0.216, 0.256) to (0.534, 0.368) due to different emission components of the Ce^{3+} and Mn^{2+} ions resulting from the energy transfer from the Ce^{3+} to Mn^{2+} ions. Moreover, CCT as another important parameter for a phosphor is calculated using the following approximate formula reported by McCamy:[42] $T = -437n^3 + 3601n^2 - 6861n + 5514.31$, where $n = (x - 0.3320)/(y - 0.1858)$. From the results listed in Table 3, one can see that the CCTs of the samples decrease dramatically with the increase of Mn^{2+} concentration. Different CCTs can meet the lighting needs for different places. When the value of y increases to 0.02, a warm-white light can be obtained with good CIE coordinates of (0.388, 0.323) and the CCT of 3284 K, which is much lower than that of the w-LEDs fabricated by the InGaN

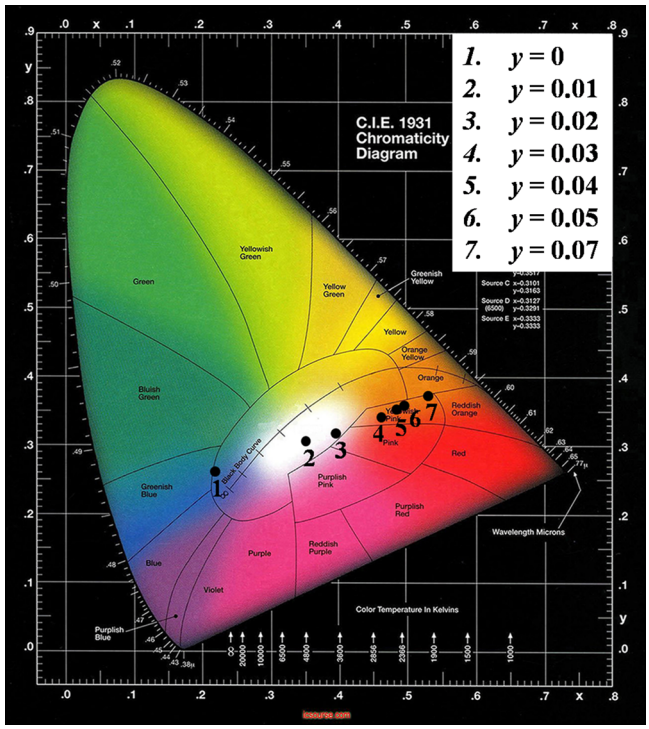

Figure 10. CIE chromaticity diagram for $CaSr_2Al_2O_6$:$0.03Ce^{3+}$, $0.03Li^+$, yMn^{2+} phosphors with different doping concentrations of Mn^{2+} ions.

chips and YAG phosphors (CCT ≈ 7750 K).[43] On the basis of the photoluminescence properties, the $CaSr_2Al_2O_6$:Ce^{3+}, Li^+, Mn^{2+} phosphor might have potential applications as a single-component white emission phosphor for UV-excited w-LEDs.

Thermal Quenching Properties of the $CaSr_2Al_2O_6$:$0.03Ce^{3+}$, $0.03Li^+$, $0.03Mn^{2+}$ Phosphor. The thermal stability of a phosphor is one of the important technological parameters for phosphors used in solid-state lighting, especially in high-power w-LEDs. To evaluate the influence of temperature on the luminescence, temperature dependence of PL spectra for $CaSr_2Al_2O_6$:$0.03Ce^{3+}$, $0.03Li^+$, $0.03Mn^{2+}$ under excitation at 358 nm is shown in Figure 11a. It can be seen that the $CaSr_2Al_2O_6$:$0.03Ce^{3+}$, $0.03Li^+$, $0.03Mn^{2+}$ phosphor shows a

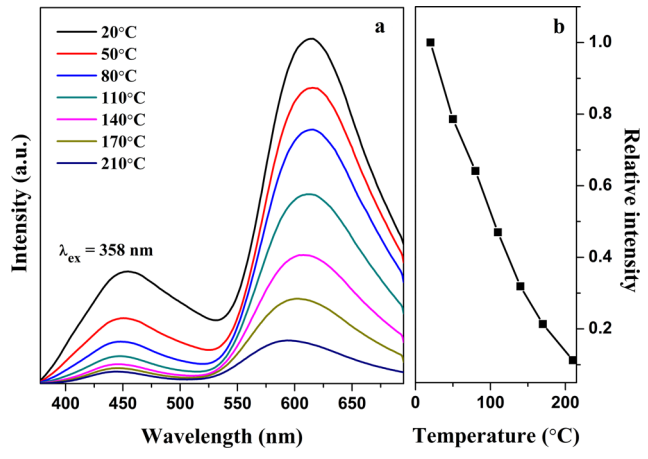

Figure 11. (a) Temperature dependence of PL spectra for $CaSr_2Al_2O_6$:$0.03Ce^{3+}$, $0.03Li^+$, $0.03Mn^{2+}$ under excitation at 358 nm. (b) Integrated intensity versus temperature.

dx.doi.org/10.1021/ic500963q | Inorg. Chem. 2014, 53, 7668−7675

relatively poor thermal stability upon heating, which needs to be further improved. The PL intensity of the $CaSr_2Al_2O_6$:0.03Ce^{3+}, 0.03Li^+, 0.03Mn^{2+} phosphor at 150 °C is only about 29% of its initial value, which can be seen from Figure 11b. The thermal quenching is caused by thermally activated crossover from the excited state to the ground state and can be explained by the thermal quenching mechanism using a configurational coordinate diagram.[44] Additionally, the emission wavelength shows slight blue shifting with increasing temperature in Figure 11a. This can be explained by thermally active phonon-assisted excitation from lower energy sublevels to higher energy sublevels in the excited states of Ce^{3+},[44] as is the same for Mn^{2+}.

CONCLUSIONS

In summary, $CaSr_2Al_2O_6$:Ce^{3+}, Li^+, Mn^{2+} phosphors have been synthesized and their luminescence properties have been investigated in detail for the first time. The $CaSr_2Al_2O_6$:Ce^{3+}, Li^+ phosphors can be efficiently excited in the wavelength range from 250 to 420 nm and have a blue emission ranging from 380 to 550 nm. By codoping the Ce^{3+} and Mn^{2+} ions into the host and utilizing the energy transfer from Ce^{3+} to Mn^{2+}, CIE coordinates of the phosphors change from (0.216, 0.256) to (0.534, 0.368) with corresponding color hues varying from blue to white and then to red. When the concentration of Mn^{2+} is increased to 0.02, a warm-white light can be obtained with the CIE coordinates of (0.388, 0.323) and the CCT of 3284 K. In $CaSr_2Al_2O_6$:Ce^{3+}, Li^+, Mn^{2+} samples, energy transfer from the Ce^{3+} to Mn^{2+} ions is a mainly resonant type via a quadrupole−quadrupole mechanism. Preliminary studies on the properties of the phosphor indicate that our identified $CaSr_2Al_2O_6$:Ce^{3+}, Li^+, Mn^{2+} phosphors might have a potential value for UV-excited *w*-LEDs.

ASSOCIATED CONTENT

Supporting Information

The XRD patterns for $CaSr_2Al_2O_6$:xCe^{3+}, xLi^+ ($0.01 \leq x \leq 0.09$) samples and the emission intensity of $CaSr_2Al_2O_6$ as a function of Ce^{3+} concentration are shown in the Supporting Information. This material is available free of charge via the Internet at http://pubs.acs.org.

AUTHOR INFORMATION

Corresponding Author

*E-mail: wyh@lzu.edu.cn. Fax: +86-931-8913554. Tel: +86-931-8912772.

Notes

The authors declare no competing financial interest.

ACKNOWLEDGMENTS

This work was supported by the National Natural Science Funds of China (Grant No. 51372105) and the Fundamental Research Funds for the Central Universities (No. lzujbky-2014-231).

REFERENCES

(1) Suehiro, T.; Hirosaki, N.; Xie, R.-J. *ACS Appl. Mater. Interfaces* **2011**, *3*, 811−816.
(2) Kim, S. K.; Lee, J. W.; Ee, H. S.; Moon, Y. T.; Kwon, S. H.; Kwon, H.; Park, H.-G. *Opt. Express* **2010**, *18*, 11025−11032.
(3) Liu, T. C.; Cheng, B. M.; Hu, S. F.; Liu, R. S. *Chem. Mater.* **2011**, *23*, 3698−3705.
(4) Mao, Z. Y.; Wang, D. J. *Inorg. Chem.* **2010**, *49*, 4922−4927.
(5) Setlur, A. A.; Heward, W. J.; Hannah, M. E.; Happek, U. *Chem. Mater.* **2008**, *20*, 6277−6283.
(6) Chen, L.; Luo, A.; Zhang, Y.; Liu, F.; Jiang, Y.; Xu, Q.; Chen, X.; Hu, Q.; Chen, S.-F.; Chen, K. J.; Kuo, H. C. *ACS Comb. Sci.* **2012**, *14*, 636−644.
(7) Wang, L.; Zhang, X.; Hao, Z.; Luo, Y.; Wang, X.; Zhang, J. *Opt. Express* **2010**, *18*, 25177−25182.
(8) Dai, P.; Zhang, X.; Bian, L.; Lu, S.; Liu, Y.; Wang, X. *J. Mater. Chem. C* **2013**, *1*, 4570−4576.
(9) Wang, M. S.; Guo, S. P.; Li, Y.; Cai, L. Z.; Zou, J. P.; Xu, G.; Zhou, W. W.; Zheng, F. K.; Guo, G. C. *J. Am. Chem. Soc.* **2009**, *131*, 13572−13573.
(10) Liu, W. R.; Huang, C. H.; Yeh, C. W.; Chiu, Y. C.; Yeh, Y. T.; Liu, R. S. *RSC Adv.* **2013**, *3*, 9023−9028.
(11) Guo, N.; Huang, Y.; Yang, M.; Song, Y.; Zheng, Y.; You, H. *Phys. Chem. Chem. Phys.* **2011**, *13*, 15077−15082.
(12) Jiao, M.; Jia, Y.; Lü, W.; Lv, W.; Zhao, Q.; Shao, B.; You, H. *J. Mater. Chem. C* **2014**, *2*, 90.
(13) Wang, X. J.; Jia, D.; Yen, W. M. *J. Lumin.* **2003**, *102−103*, 34−37.
(14) Lei, B.; Liu, Y.; Ye, Z.; Shi, C. *J. Lumin.* **2004**, *109*, 215−219.
(15) Kim, J. S.; Jeon, P. E.; Park, Y. H.; Choi, J. C.; Park, H.-L.; Kim, G. C.; Tae Whan, K. *Appl. Phys. Lett.* **2004**, *85*, 3696−3698.
(16) Liu, Y.; Zhang, X.; Hao, Z.; Wang, X.; Zhang, J. *Chem. Commun.* **2011**, *47*, 10677−9.
(17) Lian, Z.; Sun, J.; Zhang, L.; Shen, D.; Shen, G.; Wang, X.; Yan, Q. *RSC Adv.* **2013**, *3*, 16534.
(18) Li, G.; Geng, D.; Shang, M.; Peng, C.; Cheng, Z.; Lin, J. *J. Mater. Chem.* **2011**, *21*, 13334.
(19) Hou, J.; Jiang, W.; Fang, Y.; Wang, Y.; Yin, X.; Huang, F. *ECS J. Solid State Sci. Technol.* **2012**, *1*, R57−R61.
(20) Walz, L. *Z. Kristallogr.* **1998**, *213*, 47.
(21) Jiao, M.; Jia, Y.; Lu, W.; Lv, W.; Zhao, Q.; Shao, B.; You, H. *Dalton Trans.* **2014**, *43*, 3202−3209.
(22) Jiao, H.; Wang, Y. *J. Electrochem. Soc.* **2009**, *156*, J117−J120.
(23) Xia, Z.; Liu, R.-S.; Huang, K. W.; Drozd, V. *J. Mater. Chem.* **2012**, *22*, 15183.
(24) Shannon, R. D. *Acta Crystallogr.* **1976**, *32*, 751−767.
(25) Wu, Q.; Yang, Z.; Zhao, Z.; Que, M.; Wang, X.; Wang, Y. *J. Mater. Chem. C* **2014**, *2*, 4967−4973.
(26) Im, W. B.; Kim, Y. I.; Fellows, N. N.; Masui, H.; Hirata, G.; DenBaars, S. P.; Seshadri, R. *Appl. Phys. Lett.* **2008**, *93*, 091905.
(27) Dexter, D. L.; Schulman, J. H. *J. Chem. Phys.* **1954**, *22*, 1063−1070.
(28) Blasse, G. *Phys. Lett.* **1968**, *28A*, 444.
(29) Reisfeld, R.; Greenberg, E.; Velapoldi, R.; Barnett, B. *J. Chem. Phys.* **1972**, *56*, 1698−1705.
(30) Guo, N.; Huang, Y.; You, H.; Yang, M.; Song, Y.; Liu, K.; Zheng, Y. *Inorg. Chem.* **2010**, *49*, 10907−10913.
(31) Chiu, Y. C.; Huang, C. H.; Lee, T. J.; Liu, W. R.; Yeh, Y. T.; Jang, S. M.; Liu, R. S. *Opt. Express* **2011**, *19*, A331−A339.
(32) Zhou, J.; Xia, Z.; Yang, M.; Shen, K. *J. Mater. Chem.* **2012**, *22*, 21935.
(33) Haranath, D.; Mishra, S.; Yadav, S.; Sharma, R. K.; Kandpal, L. M.; Vijayan, N.; Dalai, M. K.; Sehgal, G.; Shanker, V. *Appl. Phys. Lett.* **2012**, *101*, 221905.
(34) Yu, R.; Yang, H.; Moon, B.; Choi, B.; Jeong, J. *J. Korean Phys. Soc.* **2012**, *61*, 1075−1079.
(35) Hao, Z.; Zhang, J.; Zhang, X.; Sun, X.; Luo, Y.; Lu, S.; Wang, X. *Appl. Phys. Lett.* **2007**, *90*, 261113.
(36) Shi, L.; Huang, Y.; Seo, H. J. *J. Phys. Chem. A* **2010**, *114*, 6927−6934.
(37) You, H.; Zhang, J.; Hong, G.; Zhang, H. *J. Phys. Chem. C* **2007**, *111*, 10657−10661.
(38) Guo, N.; Song, Y.; You, H.; Jia, G.; Yang, M.; Liu, K.; Zheng, Y.; Huang, Y.; Zhang, H. *Eur. J. Inorg. Chem.* **2010**, 4636−4642.
(39) Lahoz, F.; Martín, I. R.; Méndez-Ramos, J.; Núñez, P. *J. Chem. Phys.* **2004**, *120*, 6180−6190.
(40) Blasse, G. *Phys. Lett. A* **1968**, *28*, 444−445.

(41) Blasse, G.; Grabmaier, B. C. *Luminescent Materials*; Springer-Verlag: Berlin, Germany, 1994.
(42) McCamy, C. S. *Color Res. Appl.* **1992**, *17*, 142−144.
(43) Shi, Y.; Wang, Y.; Wen, Y.; Zhao, Z.; Liu, B.; Yang, Z. *Opt. Express* **2012**, *20*, 21656−21664.
(44) Dorenbos, P. *J. Phys.: Condens. Matter* **2005**, *17*, 8103−8111.